Crack Path and Branching from Small Fatigue Crack under Mixed Loading

Y. Murakami[1], K. Takahashi[2] and K. Toyama[1]

[1] Department of Mechanical Engineering Science, Kyushu University, 6-10-1 Hakozaki, Higashi-ku, Fukuoka, 812-8581, Japan, ymura@mech.kyushu-u.ac.jp
[2] Department of Energy & Safety Engineering, Yokohama National University, 79-5 Tokiwadai, Hodogaya-ku, Yokohama, 240-8501, Japan, ktaka@ynu.ac.jp

ABSTRACT. *In order to investigate the crack path of materials containing a small crack under mixed mode loading, reversed torsion and combined push-pull/torsion fatigue tests were carried out on 0.47% carbon steel specimens containing an initial small crack. The initial small cracks were introduced by a preliminary push-pull fatigue test using a specimen which contained an artificial small hole of 40μm diameter/depth. Firstly, the mechanism of fatigue crack growth under reversed torsion and combined push-pull torsion were investigated. Then, fatigue tests of push-pull followed by reversed torsion and reversed torsion followed by push-pull were carried out. Fatigue tests of combined push-pull/torsion followed by push-pull were also carried out to examine the effect of crack geometry, such as branching and kinking, on cumulative fatigue damage. Different crack growth behaviours due to different loading modes and sequences complicatedly influence the fatigue crack path and eventully the cumulative fatigue damage. Thus, existing fatigue damage theories cannot be applied to the cases presented in this study. The crack like factory-roof morphology is locally made on the fracture surface of the specimen having a semi-elliptical crack under cyclic torsion. Torsional fatigue tests of circumferentially cracked specimens were carried out to investigate the mechanism of mode III crack growth and formation of the factory-roof morphology. The factory-roof morphology in torsional fatigue of cracked specimen is formed by mode I crack branching from small semi-elliptical cracks nucleated ahead of the initial crack tip by shear.*

INTRODUCTION

The behaviours of small fatigue cracks under mixed mode loading have recently been studied by several researchers [1,2]. It has been recognized in existing literature that analyzing the path of small cracks is essential to make clear mechanical and microstructural factors affecting the fatigue strength under mixed mode loadings.

The effect of loading mode sequence has been studied by several researchers. [3-5]. It has been pointed out that the cumulative fatigue damage of torsion followed by push-pull (rotating-bending) and push-pull (rotating-bending) followed by torsion are different and cannot be predicted by Miner's rule for carbon steels [3,4] and stainless

steel [5]. The reason for deviation from Miner's rule is presumed to be the complicated behaviours of small cracks under the different loading modes and sequences.

Harada *et al.* [3] carried out sequential-fatigue tests of rotating bending and reversed torsion using a 0.24% C steel and reported that: (i) In rotating bending followed by reversed torsion, the cumulative damage (D) was in the range of 1.46 to 2.15, and (ii) in reversed torsion followed by rotating bending, D was approximately unity ($D \cong 1$). Zhang and Miller [4] carried out sequential-fatigue tests of push-pull and reversed torsion using a 0.45% C steel and reported that: (i) In the sequence of push-pull followed by torsion (PP–to–T), D was always greater than unity and $D \cong 2$ for certain conditions, and (ii) in the sequence of torsion followed by push-pull (T–to–PP), D was smaller than unity ($D<1$). However, these studies were conducted using plain specimens in which the initiation and growth behaviour of stage I cracks and growth bahaviour of stage II influence so-called fatigue damage D. Separating the influence of stage I crack and stage II crack is necessary to understand the deviation of D from 1 under various conditions.

In this paper, fatigue tests of PP–to–T and T–to–PP were carried out on 0.47% C steel specimens containing an initial small crack of 400μm in surface length. Fatigue tests of combined push-pull/torsion followed by push-pull (PP/T–to–PP) were also carried out to investigate the effects of crack geometry, such as branching and kinking from an initial small crack, on cumulative fatigue damage. Excluding the influence of initiation and growth of stage I crack, cumulative fatigue damage was studied from the viewpoint of crack propagation.

The factory roof morphology was formed on the fracture surface of the specimen having a semi-elliptical crack only when the surface length of a semi-elliptical crack was larger than ~1 mm. It has been reported by several workers that the fracture surface of mode III fatigue crack growth test specimen shows so-called "factory-roof" morphology [6,7]. However, the exact formation mechanism of factory-roof has not been made clear. Torsional fatigue tests of circumferentially cracked specimens were carried out to study the mechanism of mode III crack growth and formation of the factory-roof morphology.

EXPERIMENTAL PROCEDURES

Material

The material used was a rolled bar of 0.47% C steel (JIS S45C) with diameter of 25mm. The chemical composition of material is (wt.%): 0.47C, 0.21Si, 0.82Mn, 0.018P, 0.018S, 0.01Cu, 0.018Ni and 0.064Cr. Mechanical properties of the material are: 620MPa tensile strength, 339MPa lower yield strength, 1105MPa true fracture strength and 53.8% reduction of area.

Specimen having a small semi-elliptical surface crack

Figure 1 shows the shape and dimension of test specimen. Specimens were made by turning after annealing at 844°C for 1h. After surface finishing with emery paper,

~25μm of surface layer was removed by electro-polishing. After electro-polishing, a hole was introduced onto the surface of each specimen. The diameter of the hole, 40μm, is equal to the depth. After introducing a small hole, the specimens were annealed in a vacuum at 600°C for 1h to relieve residual stress induced by drilling. The Vickers hardness after vacuum annealing is HV=174, which is a mean value of each specimen measured at 4 points with load of 0.98N. The scatter of HV is within 5%.

A hydraulically controlled biaxial testing machine was used for both introduction of the pre-crack by push-pull and subsequent fatigue tests. Push-pull fatigue tests were conducted at σ_a = 230 MPa, in order to introduce pre-cracks of 400 μm in surface length including a hole. These tests were conducted under load control, at a frequency of 20 Hz with zero mean stress(R = -1). Specimens were annealed in a vacuum at 600°C for 1 h again to relieve the prior fatigue history by push-pull.

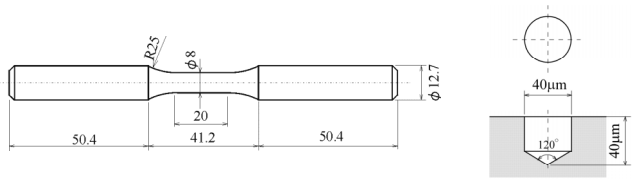

(a) (b)

Figure 1. Fatigue test specimen. (a) Shape and dimension of the specimen for reversed torsion and combined push-pull/torsion fatigue tests; dimensions in mm. (b) Artificial small hole.

Reversed torsion and combined push-pull/torsion fatigue tests

Fatigue tests under reversed torsion and combined push-pull/torsion were conducted under load control at a frequency of 12 to 20 Hz with zero shear mean stress. In order to investigate the effects of axial mean stress on the crack path, torsional fatigue tests with tensile or compressive mean stress were also carried out. The loading cycle pattern is a sine wave. In-phase combined push-pull/torsion fatigue tests were carried out at constant stress amplitude ratio, τ_a/σ_a=2.0. Plastic replicas were taken during the tests in order to monitor crack path. The fracture surfaces of specimens were observed using the scanning electron microscope (SEM).

Sequential fatigue tests

Sequential fatigue tests of push-pull, reversed torsion and combined push-pull/torsion were carried out as follows.

(a) Reversed torsion followed by push-pull. (T–to–PP)
(b) Combined push-pull/torsion in phase followed by push-pull (PP/T–to–PP)
(c) Push-pull followed by reversed torsion (PP–to–T)

Stress ranges for sequential fatigue tests were chosen so that the fatigue lives (N_f) under single loading would be in the range of $N_f = 3\times10^5$ to 4×10^5.

- Push-pull: σ_a = 191 MPa, $N_{f,pp} = 3.43\times10^5$.
- Reversed torsion: τ_a = 167 MPa, $N_{f,t} = 3.12\times10^5$.
- Combined push-pull/torsion: σ_a = 71 MPa, τ_a = 142 MPa, $N_{f,pp/t} = 3.79\times10^5$.

where $N_{f,pp}$, $N_{f,t}$ and $N_{f,pp/t}$ denote fatigue life for each loading pattern. In the subsequent discussion, *pp*, *t* and *pp/t* denote push-pull, reversed torsion and combined push-pull/torsion, respectively.

Mode III fatigue crack growth test

Figure 2(a) shows the shape and dimensions of the test specimen for the mode III fatigue crack growth test. The specimen has a circumferential notch as shown in Fig. 2(b). A hydraulically controlled biaxial testing machine was used for the introduction of the pre-crack by push-pull test and also for the torsional fatigue tests. Push-pull fatigue tests were conducted at σ_a=150 MPa, in order to introduce a pre-crack of ~200μm in depth. These specimens were annealed in a vacuum at 600°C for 1 h again to relieve the prior fatigue history introduced in push-pull fatigue test. The torsional fatigue tests were conducted under a load control condition at a frequency of 5~12Hz with zero mean stress. The loading cycle pattern is a sine wave.

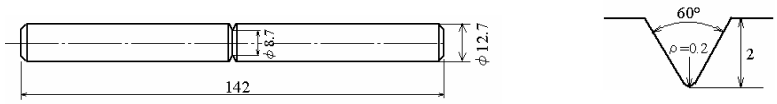

(a) (b)

Figure 2. Fatigue test specimen. (a) Shape and dimension of the specimen for mode III crack growth test (Torsional fatigue). (b) Detail of notch; dimensions in mm.

RESULTS AND DISCUSSIONS

Crack path under reversed torsion and combined push-pull/torsion

Figure 3 shows the branched cracks emanating from the initial crack tip under reversed torsion. mode I branched cracks continued propagating and led the specimen to failure. Figure 4 shows the paths of the branched cracks of broken specimens. The branched cracks which started from the initial crack tips were illustrated in the same figures, respectively, for 200μm, 400μm and 1000μm pre-cracked specimens [8]. The line of $\pm 45°$ is the direction perpendicular to the principal stresses and the line of $\pm 70.5°$ is the local maximum normal stress ($\sigma\theta_{max}$) at the crack tip.

Figure 5 shows cracks kinked by mode I from the tip of initial crack under combined push-pull/torsion. mode I cracks continued to propagate and led the specimen to failure. Figure 5(b) shows the shape and angle of kinked cracks [9]. The line of -38.0° is the direction perpendicular to the principal stresses and the line of -61.4° is the local maximum normal stress ($\sigma\theta_{max}$) at the crack tip.

The branched cracks and kinked cracks propagated eventually in a direction perpendicular to the principal stresses, though the initial branching or kinking angles are obviously larger than them and close to the direction perpendicular to the local maximum tangential stress ($\sigma\theta_{max}$) [8,9].

Murakami and Takahashi showed that the fatigue limit of pre-cracked specimens under reversed torsion [8] and combined push-pull/torsion [9] is the threshold condition for nonpropagation of mode I cracks emanating from the initial crack tip, i.e., the fatigue limit is determined by the condition for the nonpropagation of branched cracks for reversed torsion and kinked cracks for combined push-pull/torsion. Based on the fact that nonpropagating cracks under torsion and combined stress are mode I cracks, the $\sqrt{area}$ parameter model [10,11] could be applied to predict the fatigue limit [8,9].

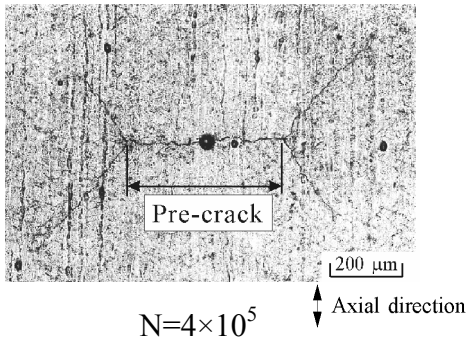

Figure 3. Propagation of branched cracks. (The 400 μm pre-cracked specimen, τ_a=152 MPa, N_f=7.9×10^5.)

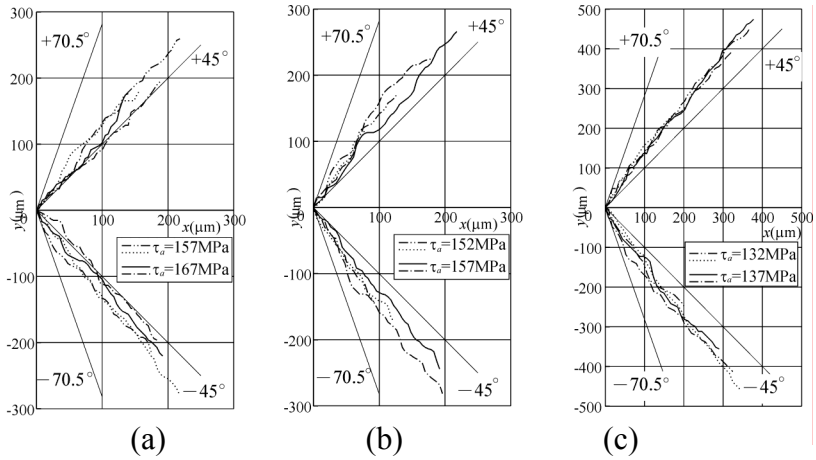

Figure 4. The shape and angle of branched cracks. (a)The 200μm pre-cracked specimen, (b)The 400μm pre-cracked specimen, (c)The 1000μm pre-cracked specimen.

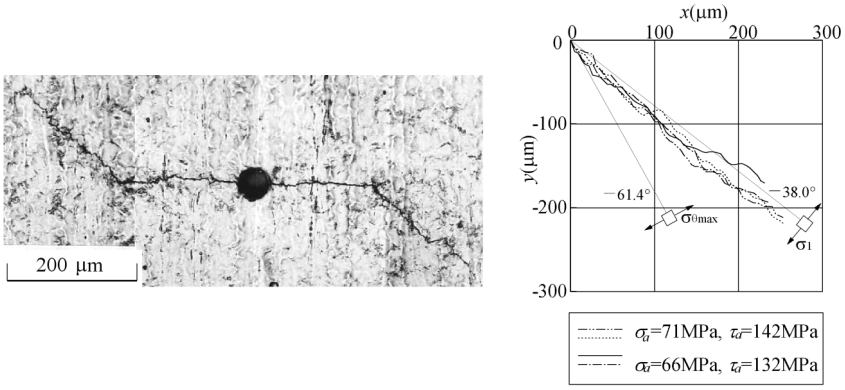

(a) (b)

Figure 5. (a) Propagation of kinked cracks under combined push-pull/torsion loadings. σ_a=71MPa, τ_a=142MPa. (b) The shape and angle of kinked cracks. The origin of the coordinate is the tip of the initial crack.

Effects of axial mean stress the on the fatigue crack path under torsional loading

In order to examine the effects of axial mean stress on the crack path, torsional fatigue tests with tensile or compressive mean stress were carried out [12]. Figures 6 and 7 show the branching of the surface cracks from an initial semi-elliptical crack by torsional fatigue with tensile and compressive mean stress, respectively.

The initial branching angle of cracks that emanated at initial crack tip was close to ±70.5° to the initial crack plane, where the cyclic component of local tangential stress $\Delta\sigma_\theta$ at the crack tip has the maximum value. The branched cracks eventually propagated perpendicularly to the plane, where the cyclic component of normal stress has the maximum value, i.e. ±45°. The paths of the branched cracks shown in Figs. 3, 6 and 7 are almost same regardless of axial mean stress. Thus, fatigue crack path is determined by the direction where the cyclic component of nominal stress has the maximum value. In other words, mean stress hardly influence the direction of fatigue crack propagation.

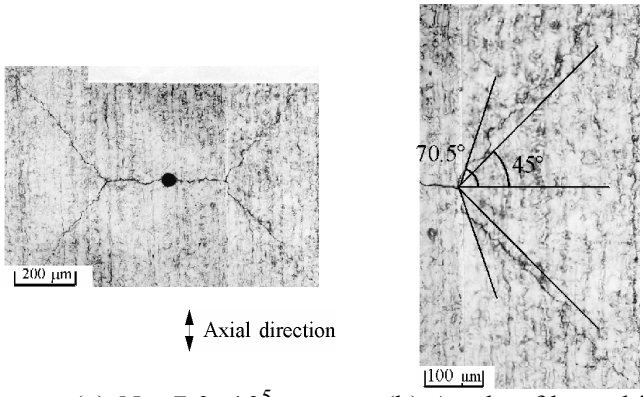

(a) N = 7.0×10^5 (b) Angle of branching

Figure 6. Propagation of the branched cracks under torsion with tensile mean stress. (σ_m=98 MPa, τ_a =142 MPa, N_f=1.0×10^6).

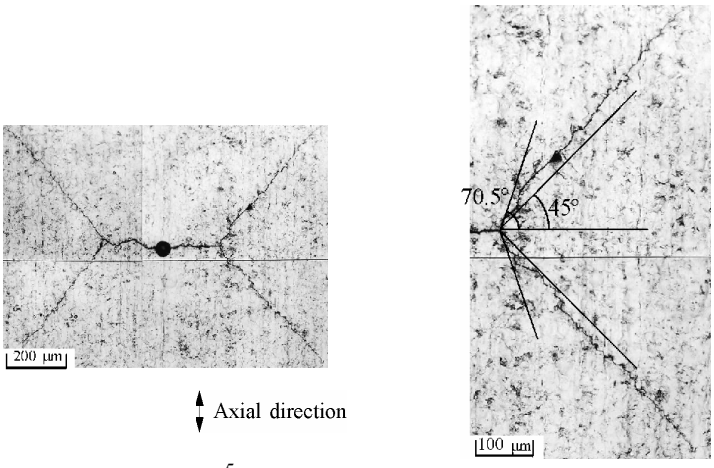

(a) $N = 3.5\times10^5$ (b) Angle of branching

Figure 7. Propagation of the branched cracks under torsion with compressive mean stress. (σ_m= -98 MPa, τ_a =162 MPa, N_f=6.7×10^5).

Ohji et al. [13] studied the path of a fatigue crack in the residual stress fields of HT80 steel. Ohji et al. indicated that the cyclic components of normal stress determined the crack path. Tanaka et al. [14] investigated the path of branched cracks under cyclic torsion with or without tensile mean stress in the medium carbon steel tubular specimen having a pre-crack of 1mm. Tanaka et al. reported that the path of branched cracks was determined by the cyclic components of normal stress. The present experimental results are consistent with those of Ohji et al. and Tanaka et al..

Effects of loading sequence on fatigue crack path

Cumulative fatigue damage

Figure 8 shows the results of so-called cumulative damage tests compared to results predicted by Miner's rule. The fraction of life in reversed torsion ($n_t/N_{f,t}$) and combined push-pull/torsion ($n_{pp/t}/N_{f,pp/t}$) is plotted against the fraction of life in push-pull ($n_{pp}/N_{f,pp}$). The fraction of life of the first loading is selected from 0.2, 0.4, 0.6 and 0.8. (In order to show the sequence of stress, the terms "the first loading" and "the second loading" will be used in this paper.) After completion of the first loading and commencement of the second loading, the fatigue tests were continued until specimen failure. The cumulative fatigue damage (D) was calculated as the summation of fractions of fatigue life of the first and second loadings. In all loading sequences, D is larger than unity ($D > 1$). In the sequence of T–to–PP, D was in the range of 1.43 to 2.13. This result of fatigue accumulation is opposite to that for plain specimens of similar materials [3,4]. In the sequence of PP/T–to–PP, D is smaller than the value of D obtained in the sequential test of T–to–PP. Therefore, D is clearly dependent on the first loading, i.e., reversed torsion or combined push-pull/torsion.

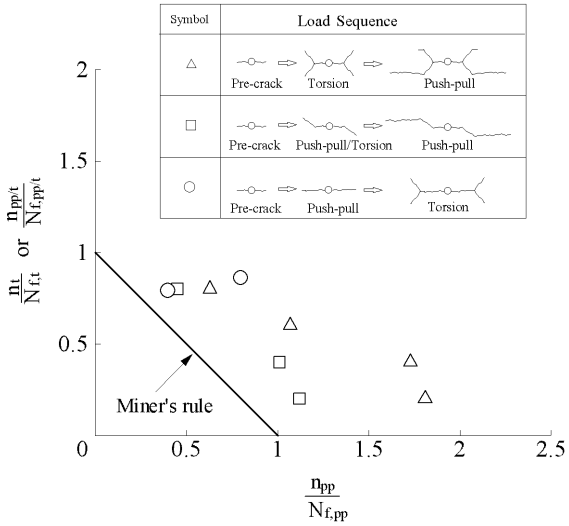

Figure 8. Fatigue test results compared to Miner's rule

Crack path in sequential fatigue tests

Figure 9(a) shows the crack path from initial crack tips under torsion. Under the subsequent push-pull, cracks started from the branched crack tips and propagated in a direction perpendicular to the specimen axis, leading the specimen to failure. Not all cracks initiating from the branched crack tips necessarily continued propagating; some stopped propagating as shown by the arrows in Fig. 9(a). The stress intensity factor at the tip of branched cracks is smaller than that of the tip of straight crack and this cause the reduction in crack growth rate when torsion is switched to push-pull. The evaluation of stress intensity factor is discussed in the next section.

Figure 9(b) shows the crack path from the initial crack in the sequence of PP/T–to–PP. Kinked cracks emanated from the initial crack tips under combined push-pull/torsion. Under the subsequent push-pull, cracks extended from the kinked crack tips. These cracks propagated perpendicular to the specimen axis and led the specimen to failure.

Figure 9(c) shows the crack path from the initial crack in the sequence of PP–to–T. Cracks initiated from the initial crack tips under push-pull and naturally propagated perpendicular to the specimen axis. After changing the loading to reversed torsion, this crack branched and propagated in the direction perpendicular to the remote maximum principal stress, i.e., ±45° to the axial direction.

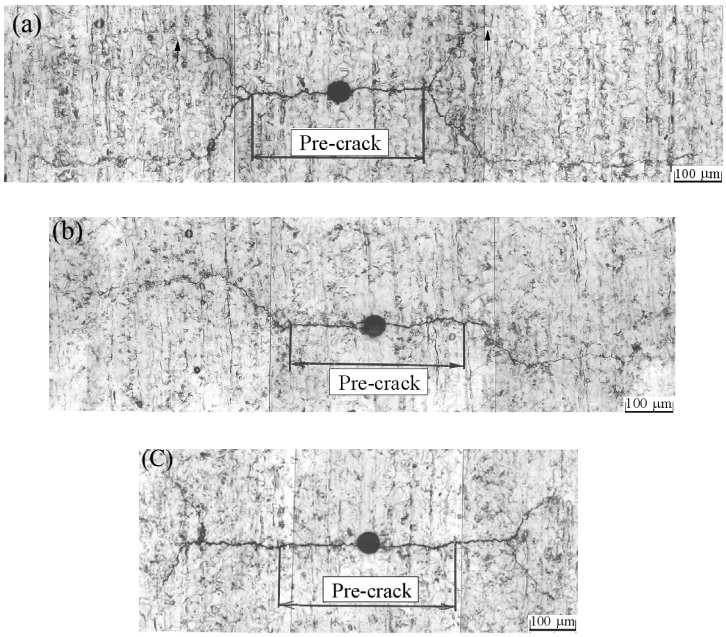

Figure 9. Crack path from the initial crack with length of 400 μm: (a) Reversed torsion with $n_t/N_{f,t}$=0.4 followed by push-pull, 3.97×10^5 push-pull cycles, $n_{pp}/N_{f,pp}$=1.16; (b) Combined push-pull/torsion with $n_{pp/t}/N_{f,pp/t}$=0.4 followed by push-pull, 1.72×10^5 push-pull cycles, $n_{pp}/N_{f,pp}$=0.5; (c) Push-pull with $n_{pp}/N_{f,pp}$=0.4 followed by torsion, 6.24×10^4 torsion cycles, $n_t/N_{f,t}$=0.2.

Crack propagation curves and fracture mechanics evaluation

Although the reality of fatigue damage of a specimen should be related to the size of crack [15], the term "fatigue damage" will be used in this paper as the value defined conventionally by Miner's rule. The fatigue damage calculated by Miner's rule will be discussed from the viewpoint of crack propagation. Figure 10 shows crack propagation curves. Crack propagation under the first loading is shown by a dotted line and crack propagation under the second loading is plotted by open marks connected with solid line. Crack length is denoted by the surface length projected onto the axial direction.

The crack propagation curves for pure push-pull or reversed torsion is also shown in Figs. 10(a) to (c). Immediately after switching from the first loading to the second loading, a reduction in crack growth rate compared to the single loading occurred, i.e., compared to push-pull in Figs.10(a) and (b) and reversed torsion in Fig. 10(c). Comparing Figs. 10(a) and (b), the reduction in the crack growth rate is larger for the sequence of T–to–PP than for PP/T–to–PP. Thus, D obtained in the sequence of T–to–PP was larger than D of PP/T–to–PP.

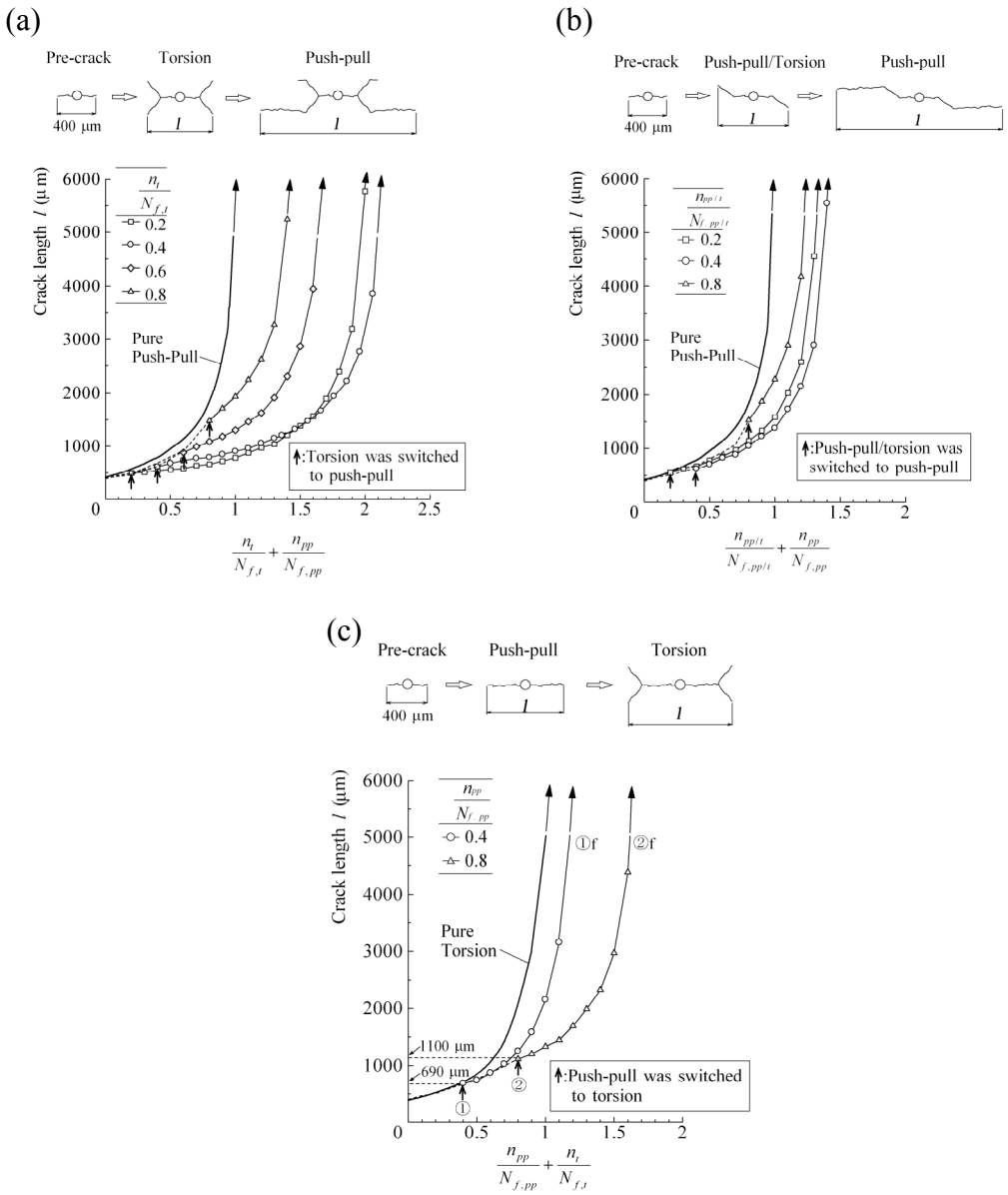

Figure 10. Crack propagation curves: (a) Reversed torsion followed by push-pull; (b) Combined push-pull/torsion followed by push-pull; (c) Push-pull followed by reversed torsion.

Figure 11 shows the variations of stress intensity factors against b/a for a two-dimensional branched crack [16] and a kinked crack [17] subjected to uniform tension. $F_{\theta\max}$ is the dimensionless correlation factor for $K_{\theta\max}$ which prescribes the local field of the maximum tangential stress ($\sigma_{\theta\max}$) at the crack tip. The measured values of b/a are also plotted in Fig. 11. $K_{\theta\max}$ of branched cracks is smaller than that of kinked cracks. The difference in the values of stress intensity factors explains why the reduction in the

crack growth rate is larger for the sequence of T–to–PP than for PP/T–to–PP. Thus, crack geometry significantly affects the conventionally defined cumulative fatigue damage. Fatigue life is almost equivalent the number of cycles spent by the small crack growth. Thus, fatigue damage should be interpreted as another expression of crack length [15].

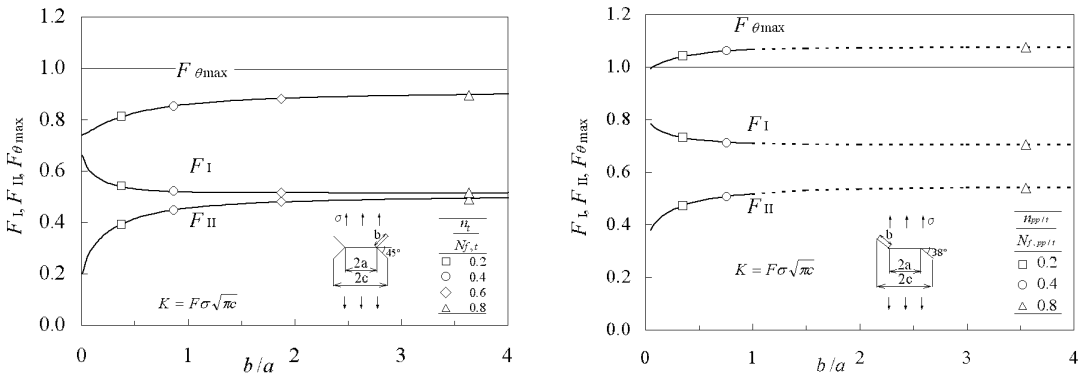

(a) (b)

Figure 11. Variation of the stress intensity factors against b/a: (a) Branched crack under uniform tension [16]; (b) Kinked crack under uniform tension [17].

Fractograph

Figure 12 shows the SEM observation of the fracture surface of a specimen subjected to PP–to–T. In Fig. 12, a factory roof morphology made by torsion is observed at the vicinity of the deepest point of the semi-elliptical crack, where the stress condition is pure mode III.

In the sequence of PP–to–T, the reduction in the crack growth rate after switching to torsion was larger in the case of $n_{pp}/N_{f,pp} = 0.8$ than for $n_{pp}/N_{f,pp} = 0.4$, as shown in Fig. 10(c). When the push-pull was switched to torsion, the crack length for $n_{pp}/N_{f,pp} = 0.4$ was 690 μm [point ① in Fig. 10(c)] and that for $n_{pp}/N_{f,pp} = 0.8$ was 1100 μm [point ② in Fig. 10(c)]. It is surprising that the remaining life of the specimen containing a crack of 1100 μm is approximately the same as that of the specimen containing a crack of 690 μm, i.e., fatigue life for $n_{pp}/N_{f,pp} = 0.4$ was 2.46×10^5 [①→①f in Fig. 10(c)] and fatigue life for $n_{pp}/N_{f,pp} = 0.8$ was 2.50×10^5 [② →②f]. This may be due to the difficulty of crack growth at the deepest point of the crack, where the crack forms a factory roof. The effective stress intensity factor is considered to be reduced because of the interference of the crack surfaces [7].

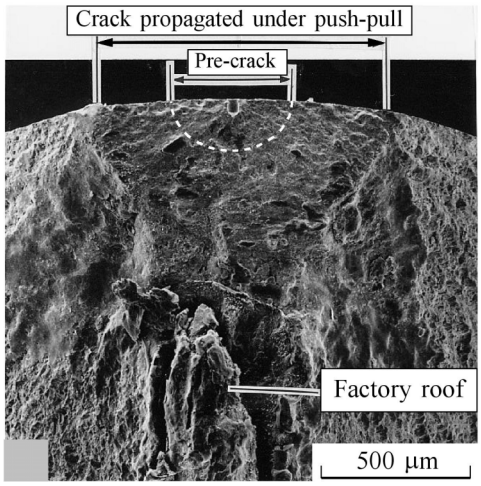

Figure 12. SEM observation of the fracture surface: Push-pull with $n_{pp}/N_{f,pp}$ = 0.8 followed by torsion.

Crack path under mode III loading

Fractographic investigation

Figure 13(a) shows macroscopic mode III fracture surface of the specimen tested at ΔK_{III} = 11.5 MPa√m . The fracture surface presents a typical morphology of the factory roof. Figure 13(b) shows the mechanism of the formation of the factory roof [18]. Prior to the formation of factory roof, many small semi-elliptical cracks are nucleated by mode III loading ahead of the initial circumferential crack tip as shown in Fig.14. Contrary to these cases of low ΔK_{III}, a totally flat fracture surface was produced in the specimen tested at high ΔK_{III} such as ΔK_{III} =17.3 MPa√m [18].

Formation mechanism of factory roof

The profile of factory-roof was investigated by slicing and polishing the mode III specimens as schematically shown in Fig.15(a). Then, specimens were etched with a nital. As shown in Fig.15(b), a branching of cracks was observed. The number of branched cracks increases as the surface layer is removed more as shown in Fig. 15(c).

The profile of factory-roof in Fig. 15(c) is very similar to that of the branched cracks in Fig. 3. The branching angle in Fig. 15(b) is also larger than ±45° and rather close to ±70.5°. Figure 16 schematically shows the formation mechanism of factory-roof. The mechanism explained in Fig. 16 is substantially identical to that of Fig. 3. Thus, the formation mechanism of factory-roof at the circumferential crack tip or notch root is presumed to be the same as the case of a small semi-elliptical surface crack.

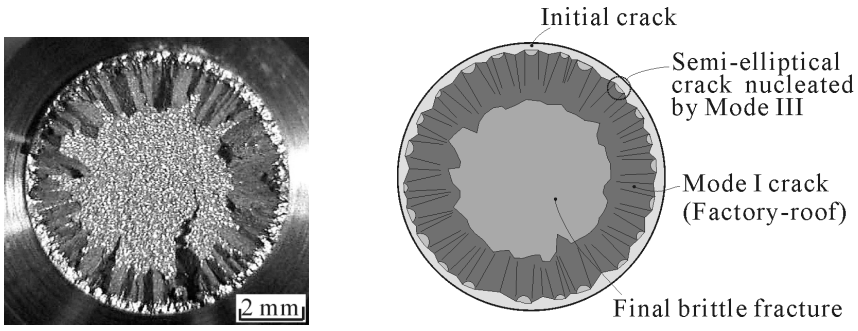

(a) (b)

Figure 13. (a)Fracture surface of the circumferentially cracked specimen, τ_a = 132 MPa , ΔK_{III}=11.5 MPa√m. (b) Formation mechanism of the factory roof.

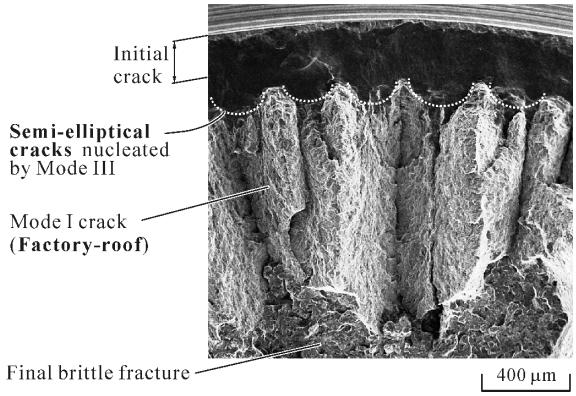

Figure 14. Fracture surface of the circumferentially cracked specimen, τ_a = 132 MPa, ΔK_{III}=11.5 MPa√m. Many small semi-elliptical cracks nucleated by mode III ahead of the initial circumferential crack tip prior to the formation of factory-roof.

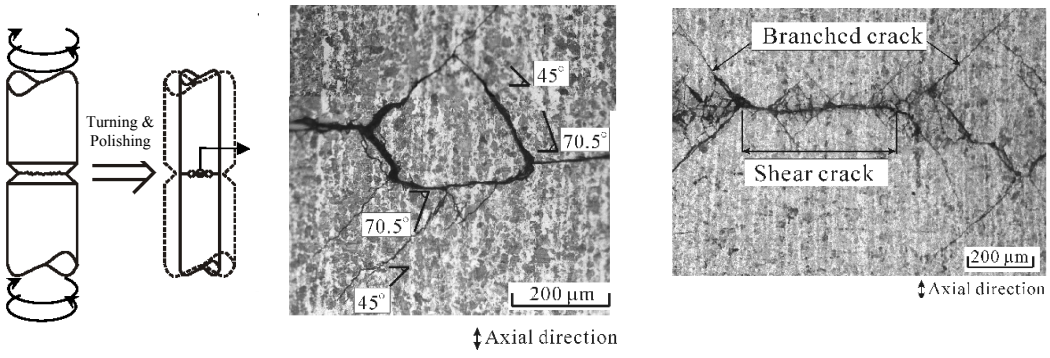

(a) (b) (c)

Figure 15. Profiles of cracks under mode III loading, ΔK_{III}=13.6 MPa√m, τ_a=142 MPa. (a) Slicing and polishing the mode III specimens Formation mechanism of "factory-roof". (b) Angle of branched cracks, crack depth 260μm. (c) Shape of factory-roof crack, crack depth 530μm.

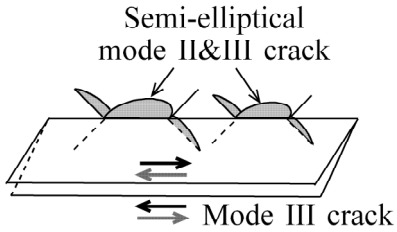

Figure 16. Formation mechanism of factory-roof.

CONCLUSIONS

(1) Mode I branched cracks and kinked cracks emanated from the initial semi-elliptical surface crack tip under reversed torsion and combined push-pull/torsion. The mode I cracks propagated eventually in a direction perpendicular to the remote principal stresses, though the initial branching and kinking angles are obviously larger than them and close to the direction perpendicular to the local maximum tangential stress ($\sigma\theta$max).

(2) The path of branched cracks under torsional loading is determined by the direction where the cyclic component of nominal stress has the maximum value, i.e. the mean stress does not influence the fatigue crack growth direction.

(3) In all loading sequences of this study, in which specimens with an initial small surface crack were used, the fatigue damages (D) based on Miner's rule were larger than unity. Deviation from Miner's rule was largest in the sequence of reversed torsion followed by push-pull.

(4) Unpredictably complicated fatigue crack path can be made depending on the combination of loading modes (mode I, II and III) and loading sequences. Such complicated fatigue crack path causes deviation from Miner's rule.

(5) The factory-roof morphology in torsional fatigue of cracked specimen is formed by mode I crack branching from small semi-elliptical cracks nucleated ahead of the initial crack tip by shear.

REFERENCES

1. Brown, M.W. and Miller, K.J. (1989) *Biaxial and Multiaxial Fatigue*, Mech. Engng Publ. Ltd., London.
2. Socie, D.F. and Marquis, G.B. (2000) *Multiaxial Fatigue*, Society of Automotive Engineers, Inc., Warrendale, Pa.
3. Harada, S., Endo, T. and Shimizu, Y. (1987) *Trans. Jpn. Soc. Mech. Engrs* **A53** (487), 369-377.
4. Zhang, W. and Miller, K. J. (1996) *Fatigue Fract. Eng. Mater. Struct.*, **19**, 229-239.
5. Weiss, J. and Pineau, A. (1993) *Metallurgical Trans.* A **24A**, 2247-2261.
6. Pook, L. P. and Sharples, J. K. (1979) *Int. J. Fract*. **15**, R223-226.
7. Ritchie, R.O., McClintock, F.A., Nayeb-Hashemi, H. and Ritter, M.A. (1982) *Metal.*

Trans. **13A**, 101-110.
8. Murakami, Y. and Takahashi, K. (1998) *Fatigue Fract. Engng Mater. Struct.* **21,** 1473-1484.
9. Murakami, Y. and Takahashi, K. (1998) In: *Proc. 12th Biennial Conference on Fracture, ECF 12,* **1**, pp. 67-72. EMAS publishing.
10. Murakami, Y and Endo, M. (1994) *Int. J. Fatigue* **16**, 163-182.
11. Murakami, Y. (2002) *Metal Fatigue: Effects of Small Defects and Nonmetallic Inclucions,* Elsevier Science Ltd., Oxford.
12. Takahashi, K and Murakami, Y. (2002) *Trans. Jpn. Soc. Mech. Engrs* **A68** (668), 645-652.
13. Ohji, K., Tsuji, M., Kubo, S., Ono, Y., Yawata, A., Umei, K. (1993) *Trans. Jpn. Soc. Mech. Engrs* **A59** (562), 1492-1436.
14. Tanaka, K., Akiniwa, Y., Mikuriya, T. Tanaka, K. and Kimachi, H. (2001) In: Proc. 6th Int. Conference Biaxial/Multiaxial Fatigue & Fracture, vol.2, p.683.
15. Murakami, Y., Harada, S., Endo, T., Tani-isi, H. and Fukushima, Y. (1983) *Eng. Fract. Mech.* **18**, 909.
16. Vitek, V. (1977) *Int. J. Fract.* **13**, 481-501. In: *Stress Intensity Factors Handbook* **2** (1987) Y. Murakami et al. (Eds.), pp. 386-387. Pergamon Press.
17. Kitagawa, H. and Yuuki, R. (1978) *Trans. Jpn. Soc. Mech. Engrs* **44**(386), 3346-3353. In: *Stress Intensity Factors Handbook* **2** (1987) Y. Murakami et al. (Eds.), pp. 362-363. Pergamon Press.
18. Takahashi, K. and Murakami, Y. (2001) In: Proc. 6th Int. Conference Biaxial /Multiaxial Fatigue & Fracture, vol.2, p.581.